scientific reports



OPEN Cerebral perfusion metrics calculated directly from a hypoxia-induced step change in deoxyhemoglobin

James Duffin^{1,2™}, Ece Su Sayin¹, Olivia Sobczyk^{2,3}, Julien Poublanc³, David J. Mikulis³ & Joseph A. Fisher^{1,2,4}

Resting cerebral perfusion metrics can be calculated from the MRI ΔR_2 * signal during the first passage of an intravascular bolus of a Gadolinium-based contrast agent (GBCA), or more recently, a transient hypoxia-induced change in the concentration of deoxyhemoglobin ([dOHb]). Conventional analysis follows a proxy process that includes deconvolution of an arterial input function (AIF) in a tracer kinetic model. We hypothesized that the step reduction in magnetic susceptibility accompanying a step decrease in [dOHb] that occurs when a single breath of oxygen terminates a brief episode of lung hypoxia permits direct calculation of relative perfusion metrics. The time course of the ΔR_2 * signal response enables both the discrimination of blood arrival times and the time course of voxel filling. We calculated the perfusion metrics implied by this step signal change in seven healthy volunteers and compared them to those from conventional analyses of GBCA and dOHb using their AIF and indicator dilution theory. Voxel-wise maps of relative cerebral blood flow and relative cerebral blood volume had a high spatial and magnitude congruence for all three analyses (r > 0.9) and were similar in appearance to published maps. The mean (SD) transit times (s) in grey and white matter respectively for the step response (7.4 (1.1), 8.05 (1.71)) were greater than those for GBCA (2.6 (0.45), 3.54 (0.83)) attributable to the nature of their respective calculation models. In conclusion we believe these calculations of perfusion metrics derived directly from ΔR_2^* have superior merit to calculations via AIF by virtue of being calculated from a direct signal rather than through a proxy model which encompasses errors inherent in designating an AIF and performing deconvolution calculations.

Keywords Cerebrovascular, Cerebral blood flow, Mean transit time, Cerebral blood volume, Magnetic resonance imaging, Hypoxia, Deoxyhemoglobin

Abbreviations

AIF Arterial input function ANOVA Analysis of variance **FRC** Functional residual capacity **GBCA** Gadolinium-based contrast agents MTT Mean transit time

PCO₂ Partial pressure of carbon dioxide

 PO_2 Partial pressure of oxygen

PaO₂ Partial pressure of oxygen in arterial blood

rCBF Relative cerebral blood flow rCBV Relative cerebral blood volume The ΔR_2^* signal in a voxel

SaO₂ Arterial hemoglobin oxygen saturation THx-dOHb Transient hypoxia-induced deoxyhemoglobin

¹Department of Physiology, University of Toronto, Toronto, ON, Canada. ²Department of Anaesthesia and Pain Management, University Health Network, Toronto, Canada. 3 Joint Department of Medical Imaging and the Functional Neuroimaging Laboratory, University Health Network, Toronto, Canada. ⁴Toronto General Hospital Research Institute, University Health Network, University of Toronto, Toronto, Canada. [™]email: j.duffin@ utoronto.ca

THx-dOHb-AIF
THx-dOHb-Step
Transient hypoxia-induced deoxyhemoglobin analyzed using an arterial input function
Transient hypoxia-induced deoxyhemoglobin analyzed using the step reoxygenation
(recovery)

Dynamic susceptibility contrast magnetic resonance perfusion imaging interrogates the voxel-wise passage of a bolus of a susceptibility contrast agent such as a gadolinium-based contrast agent (GBCA), to measure resting cerebral perfusion metrics including relative cerebral blood flow (rCBF), relative cerebral blood volume (rCBV), and mean capillary transit time (MTT). Analysis of GBCA data for hemodynamic measures follows a vascular model-based approach requiring the deconvolution of a tissue concentration time series with a measured arterial input function (GBCA-AIF analysis) 1 . The AIF is based on the strength and temporal evolution of a ΔR_2^* signal, sampled in an arterial region of interest such as the middle cerebral artery $^{2-4}$ or choroid plexus 5 where the voxel may be entirely contained in the vessel.

Recent reports describe the use of transient hypoxia-induced changes in deoxyhemoglobin concentration (THx-dOHb) as an endogenously-generated contrast agent $^{6-13}$. Changes in arterial deoxyhemoglobin concentrations ([dOHb]) are produced by targeting the alveolar partial pressures of oxygen (PO₂) via changes in the PO₂ of inspired gases $^{14-17}$. The calculation of resting perfusion metrics using THx-dOHb as a contrast agent is similar to that for GBCA, i.e. an indicator dilution method 18 with an AIF (THx-dOHb-AIF). This analysis calculates the concentration of contrast agent in the voxel via the deconvolution of the tissue signal with an AIF. THx-dOHb-AIF analysis has been shown to generate resting perfusion metrics that are comparable to those obtained using GBCA-AIF analysis in healthy participants 11 , patients with steno-occlusive disease 19 , and patients with brain tumors 20 .

For the reoxygenation phase, there is a remarkable anatomical-physiological feature that enables full saturation of the pulmonary venous blood in a *fraction of a second* (Fig. 1). During an inspiration, inhaled gas passes down successive generations of branches of bronchi and alveolar ducts while undergoing minimal gas exchange. But, in the fraction of a second that the inspired gas passes the 16th branch of airways into the alveolae where most of the gas exchange takes place, the surface area for oxygen diffusion expands from 225 cm² to 130 m², resulting in a near instantaneous change in the oxygen partial pressure of the pulmonary capillary blood.

Breathing a suitably hypoxic gas can maintain pulmonary venous, and thus arterial PO_2 at, for example, 40 mmHg^{14} , equivalent to an SaO_2 about 75%. During a single inspiration of oxygen-enriched air, the pulmonary alveoli, and thus alveolar capillary blood, undergo abrupt oxygen saturation. The blood which has suddenly increased its SaO_2 is conducted into the pulmonary vein, left atrium and ventricle, and enters the arterial tree, retaining the same abrupt leading edge of hemoglobin saturation at every branching as the vessels ramify into the brain. This rapid transition from deoxyhemoglobin to oxyhemoglobin describes a susceptibility contrast agent step function²². We proposed to examine whether the resulting decrease in the ΔR_2^* signal could be used to directly calculate resting perfusion metrics.

The simplifying assumption for the analysis of step changes in [dOHb] (THx-dOHb-Step) is that the ΔR_2^* signal (S) in a voxel is directly proportional to [dOHb]²³ or $(1-SaO_2)^{8,12}$. Equation (1) sets out this proportionality.

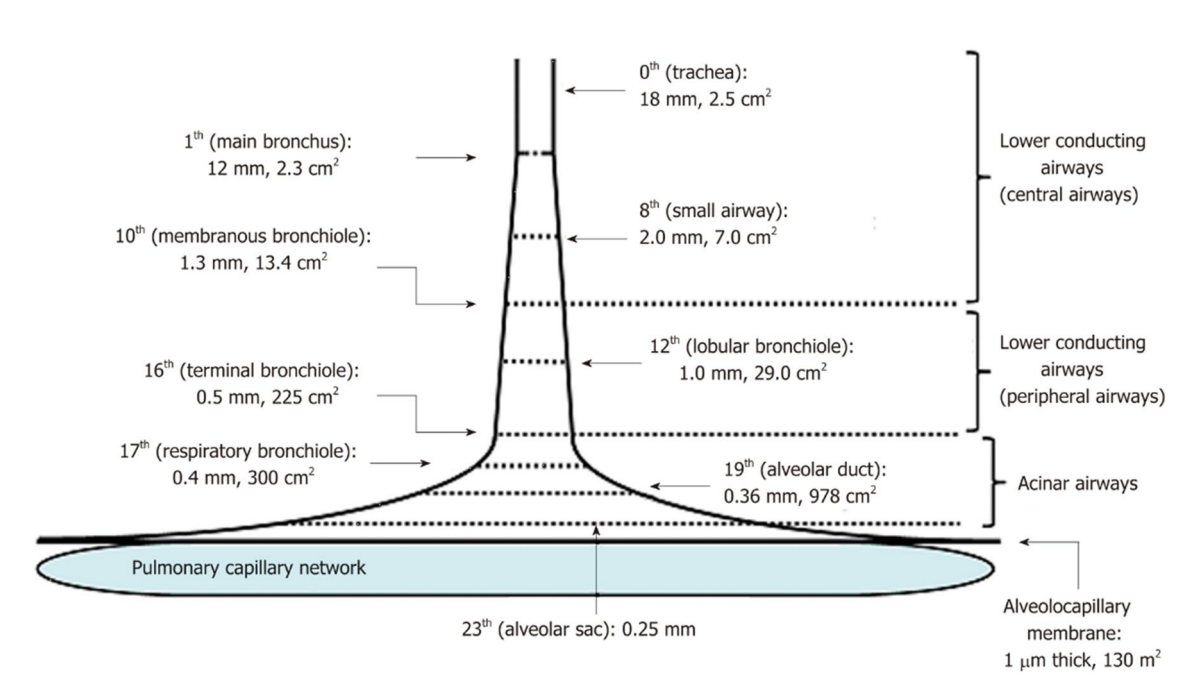


Figure 1. Trumpet or thumbtack model. Schematic presentation of effective diameter and cross-sectional area along lower conducting airways and acinar airways (Figure from Yamaguchi et al.²¹ distributed under the Creative Commons Attribution Non-Commercial (CC BY-NC 4.0) license).

$$S = C \times [Hb] \times (1 - SaO_2) \times CBV \tag{1}$$

where S, the ΔR_2^* signal in a voxel; C, a proportionality constant; CBV, the volume of blood in a voxel; SaO₂, the arterial oxygen saturation; [Hb], the arterial hemoglobin concentration (assumed to be 130 g/L unless measured). SaO₂ is related to arterial PO₂ (PaO₂) by the in-vivo oxygen dissociation curve²⁴. Equation (2) describes the relation

$$S_a O_2 = \frac{K \times PO_2^n}{\left(1 + K \times PO_2^n\right)} \tag{2}$$

where n and K are derived from a Levenburg-Marquardt fit to measured human data²⁴:

$$K = 5 \times 10^{-142} \times (pH)^{157.31}$$

$$n = -4.4921 \times pH + 36.365$$

pH is assumed to be 7.4 unless measured.

A step increase in alveolar PO₂, from approximately 40 to 95 mmHg, produces a step increase in SaO₂ from 75 to 97%. The change in signal as oxygenated blood displaces the deoxygenated blood in the voxel reflects the hemodynamic parameters of the voxel, which it is our intent to measure.

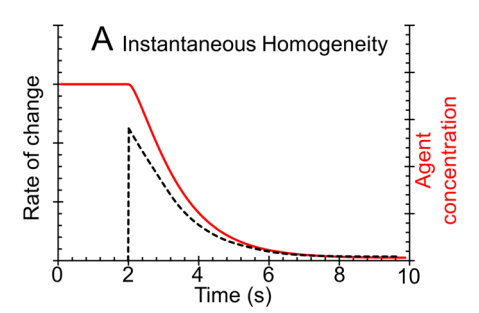
Current models for voxel-wise analysis of hemodynamics

The two models commonly used to describe the process of displacement of one indicator with another are illustrated in Fig. 2. If the voxel is viewed as a compartment, the contents of which undergo instantaneous mixing with the inflowing indicator²⁵ as illustrated in Fig. 2A, the signal intensity response to a step change in susceptibility contrast agent such as dOHb reflects the balance of contrast agent in the course of the exchange. In the case of a high [dOHb] in the voxel and a low [dOHb] in the inflow, the initial high rate of signal intensity decline falls off exponentially as the difference in inflow and outflow of contrast declines to zero. The time constant of this exponential is MTT. Thus, model Fig. 2A describes the central volume theorem where MTT = CBV/CBF. This is a generic kinetic model for unknown patterns of blood flow through the tissues and is applied for the calculation of perfusion metrics using the GBCA-AIF and THx-dOHb-AIF analyses⁸.

Alternatively, if the displacement of the high susceptibility contrast such as dOHb in the voxel is viewed as a filling of a population of capillaries with varying transit times²⁶, then the rate of decrease of the signal intensity response is attributed to the distribution of the blood with reduced [dOHb] to an assumed bundle of capillaries having a normal distribution of blood transit times (Fig. 2B). As blood with decreased [dOHb] simultaneously enters the voxel's population of capillaries, the signal intensity decreases linearly until capillaries with shortest transit times are filled with the decreased contrast agent. Thereafter the rate of decline of the signal intensity slows as oxygenated blood progressively replaces deoxygenated blood in the voxel.

Direct analysis model

The GBCA AIF and THx-dOHb-AIF analyses use the kinetic model with first order dynamics shown in Fig. 2A. In that case the residue function is an exponential curve with a time constant MTT as stated in "Methods" Eq. (4). However, it is unlikely this simple model describes the physiological events sufficiently to be the basis for the analysis of the ΔR_2^* signal response to a step decrease in [dOHb]. Indeed, in examining the step response patterns of the ΔR_2^* signal during reoxygenation in multiple voxels with little noise we noted that, despite generating a near instantaneous initial step change in susceptibility contrast agent proximally in the major arteries, at the voxel level, most voxels had a period of initial acceleration of signal decline. This was followed by a period of



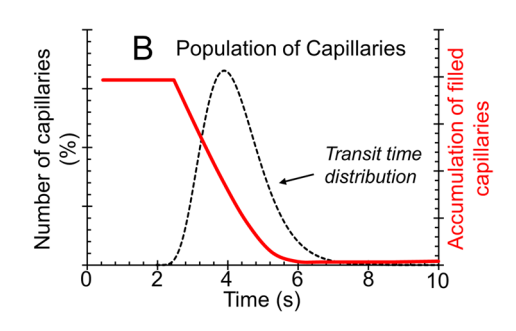


Figure 2. Step response models. (**A**) Instantaneous Homogeneity. Blood with decreased contrast agent [dOHb] enters a well-mixed container, so that the initial high rate of decrease of [dOHb] is a declining exponential (dashed line), approaching an asymptote (red line). (**B**) Population of Capillaries: Blood with decreased contrast agent [dOHb] enters the voxel capillary population simultaneously, initially perfusing all capillaries, producing a linear decline in net voxel [dOHb] (red line) proportional to the blood flow into the voxel. Capillaries with progressively longer transit times continue to fill with oxygenated blood, resulting in an exponential decline in the net [dOHb] to an asymptote (red line).

linear decrease, ending with a period where the rate of decline decelerated to zero. Note that models 2A and 2B have their maximal rate of decline at the beginning. Model 2B begins with a sudden transition from zero change in contrast agent, to a constant rate of decline, decelerating to a steady value.

We propose that a modified version of the model described by Jesperson et al. 26 is suitable to explain the observed ΔR_2^* signal response to a step increase in SaO_2 . The contrast agent accumulation dynamics in a voxel can be viewed as the result of a distribution of contrast agent entry times in a population of capillaries, rather than the synchronous entry assumed in Fig. 2B and Fig. 1 in Jespersen et al. 26 . Even with the assumption of a step increase in hemoglobin oxygenation in all vessels, the arrival time of the saturation wavefront will vary among vessels entering the voxel as there is a range of blood flows and path distances to the voxel. This model is illustrated in Fig. 3. Once all vessels entering the voxel contain oxygenated blood, the ΔR_2^* signal will decline linearly until the saturation wavefront of oxygenated blood in some vessels begins to leave the voxel. At that stage there is an exponentially decreasing rate of decline in the ΔR_2^* signal, reaching an asymptote at a new steady signal value.

We propose to measure perfusion metrics directly from measurements of the ΔR_2^* signal response to the step increase in SaO₂, assuming the descriptive model shown in Fig. 3: the THx-dOHb-Step analysis. We demonstrate that this direct examination of the ΔR_2^* signal step response enables the calculation of relative perfusion metrics without recourse to conventional deconvolution analysis and selection of an AIF and kinetic model. Here we compare our proposed THx-dOHb-Step analysis perfusion metrics to those generated from GBCA-AIF and THx-dOHb-AIF analyses using the instantaneous homogeneity kinetic model⁸ (Fig. 2A), in seven healthy study participants. This comparison is necessarily qualitative, as the comparator proxy measures are not considered gold standard hemodynamic measures.

Results

Reoxygenation signal noise Figure 4 illustrates the variation in the AR * signal noise among

Figure 4 illustrates the variation in the ΔR_2^* signal noise among voxels and shows how the fitting of a Gompertz function is used to provide a best fit to the data.

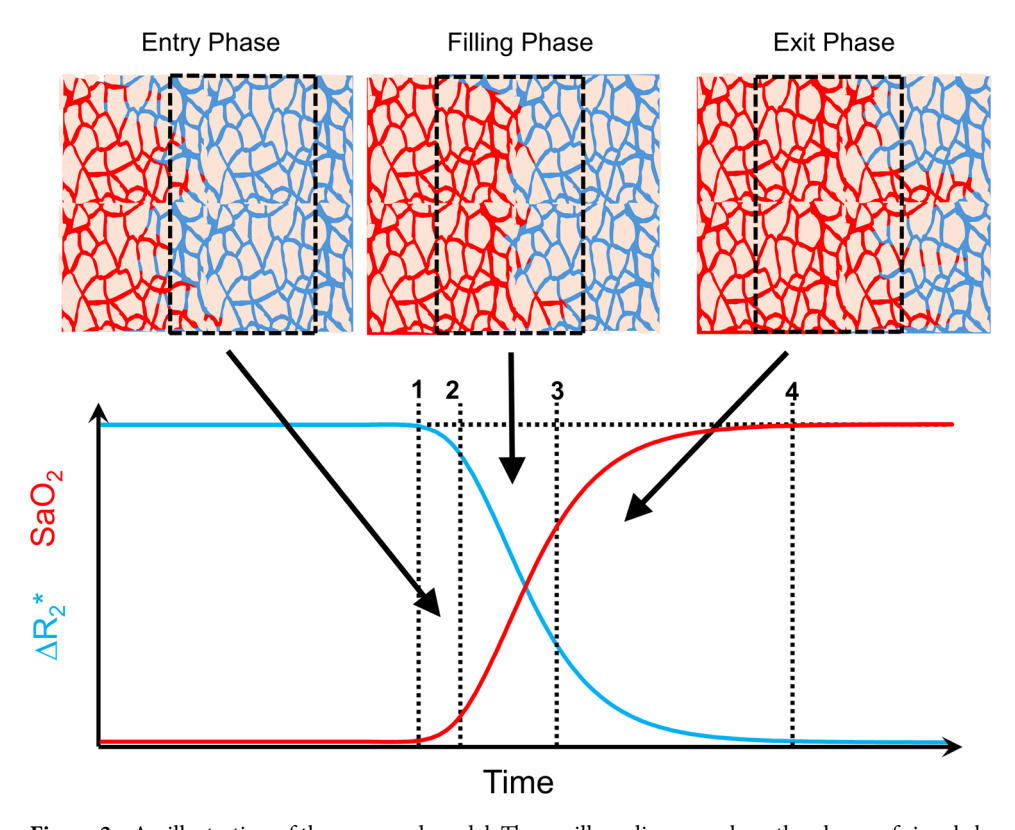


Figure 3. An illustration of the proposed model. The capillary diagrams show the phases of signal change as the wavefront of the step increase in SaO_2 in a population of vessels passes through a voxel to fill all vessels in the voxel with blood containing increased SaO_2 . The graph shows the net increase in SaO_2 within the voxel (red line) and the resulting ΔR_2^* signal (blue line) as the step change in SaO_2 in the population of capillaries reaches the voxel. At dotted line 1 in the graph, the entry phase illustrates the arrival of oxygenated blood (red) displacing the hypoxic blood (blue). Entry is complete in all capillaries at dotted line 2 in the graph and the filling phase is a constant rate of filling with oxygenated blood in all vessels, resulting from a net voxel flow of CBF and a linear decrease in ΔR_2^* signal. At dotted line 3 in the graph, the linear stage of filling ends and the exit phase is characterized by the slowing of the net rate of increase in SaO_2 with ΔR_2^* signal following a declining exponential pattern reaching an asymptote of zero change at dotted line 4.

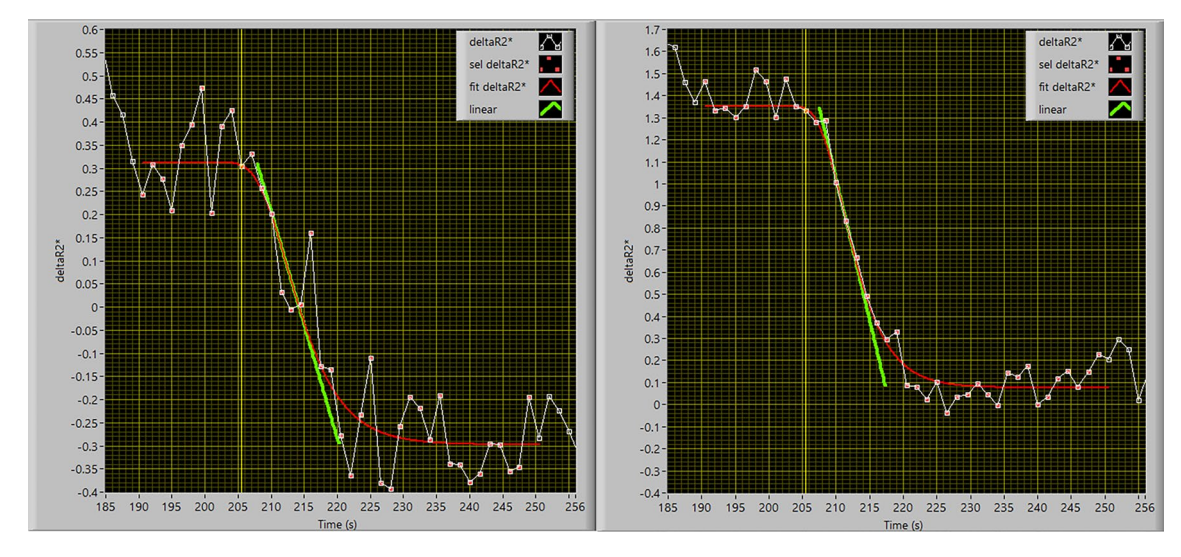


Figure 4. ΔR_2^* signal during reoxygenation in 2 voxels with different levels of noise. The images are screen captures from the step analysis computer program. The image on the left is representative of a noisy signal, with the image on the right a less noisy signal. The red line is the fit of the Gompertz function to the ΔR_2^* signal response to a step change in SaO₂. The green line is fitted to the linear portion of the function and extended to baseline (top) and asymptote of oxygenated blood (bottom). The vertical yellow line is the reference time cursor used for all voxels to calculate blood arrival time. (The analysis method is described in "Methods" Fig. 11).

Group comparisons

Figure 5 compares the group averaged metrics from the three analyses in the healthy participants using boxplots and Fig. 6 shows scatter and Bland–Altman plots. Supplemental table 1 provides all perfusion metrics for all subjects and all three analyses. Figure 7 displays axial slices of the group averaged perfusion metrics and their associated GM and WM histograms.

The grouped mean (SD) hemodynamic ratios for GM to WM are presented in Table 1. The GBCA- AIF rCBV GM to WM ratio was significantly lower than those for THx-dOHb-AIF and THx-dOHb-Step (P = 0.013 and 0.018 respectively), while the GM to WM ratios for MTT and rCBF did not differ between analyses.

A two-way ANOVA of MTT values with factors GM to WM ratio and type of analysis found that the MTT values for the THx-dOHb-Step analysis were greater in WM than GM for all three analyses (P = 0.016). MTT values for the THx-dOHb-Step analysis were greater than those for the other two analyses (P < 0.001), which did not differ (P = 0.971).

Discussion

The main findings of this study are that the hemodynamic parameters obtained by the analysis of the voxel ΔR_2^* changes following a step reoxygenation produced similar distributions of relative hemodynamic measures obtained using GBCA and THx-dOHb contrasts analyzed using existing kinetic model-based deconvolution analysis involving an AIF. We believe the similarity of the patterns of the hemodynamic measures implies widespread correspondence throughout the brain of the relative blood flow and volume. Nevertheless, the strongest arguments supporting the hypothesis of validity of the THx-dOHb-Step method are the full visual and mathematical traceability of the process from signal detection to hemodynamic calculation, and the physiological authenticity of the vascular model it follows (Fig. 3).

Group metrics for rCBF and rCBV

The resting perfusion group metrics for rCBF and rCBV for all three analyses are relative measures. Consequently, comparisons to published absolute values are not possible, leaving only comparisons of similarity of distribution to relative values measured by deconvolution and AIF. The group averaged maps of rCBV and rCBF in Fig. 7 show similar patterns of distribution of their measured parameters, which are corroborated in the scatter and Bland–Altman plots in Fig. 6. Of particular significance is that they are also strikingly similar in regional distribution to published group average maps of these metrics generated using other analytical methods^{13,27–31}.

The GM to WM ratios for rCBF and rCBV were compared between analysis techniques and found that the GM to WM ratio for rCBF did not differ between analysis techniques. GM to WM ratios for rCBF reported in the literature range from 2:1 to 3:1 in healthy participants. One study found the GM to WM ratio to be 3.34 ± 0.48 to 1 when using CT perfusion, and about 2.78 ± 0.25 to 1 when using PET³². This finding indicates that rCBF is significantly higher in grey matter compared to white matter, and is consistent with the findings of the current study. The GM to WM ratios for GBCA-AIF rCBV were significantly lower than those for THx-dOHb-AIF and THx-dOHb-Step analyses (P = 0.013 and 0.018 respectively). The GM to WM ratio for rCBV calculated using THx-dOHb match literature values of about 2 to 1 in healthy participants. However, the rCBV GM to WM ratio calculated using GBCA is slightly lower (ratio of 1.5 to 1) in comparison to published literature values (~ 2 to

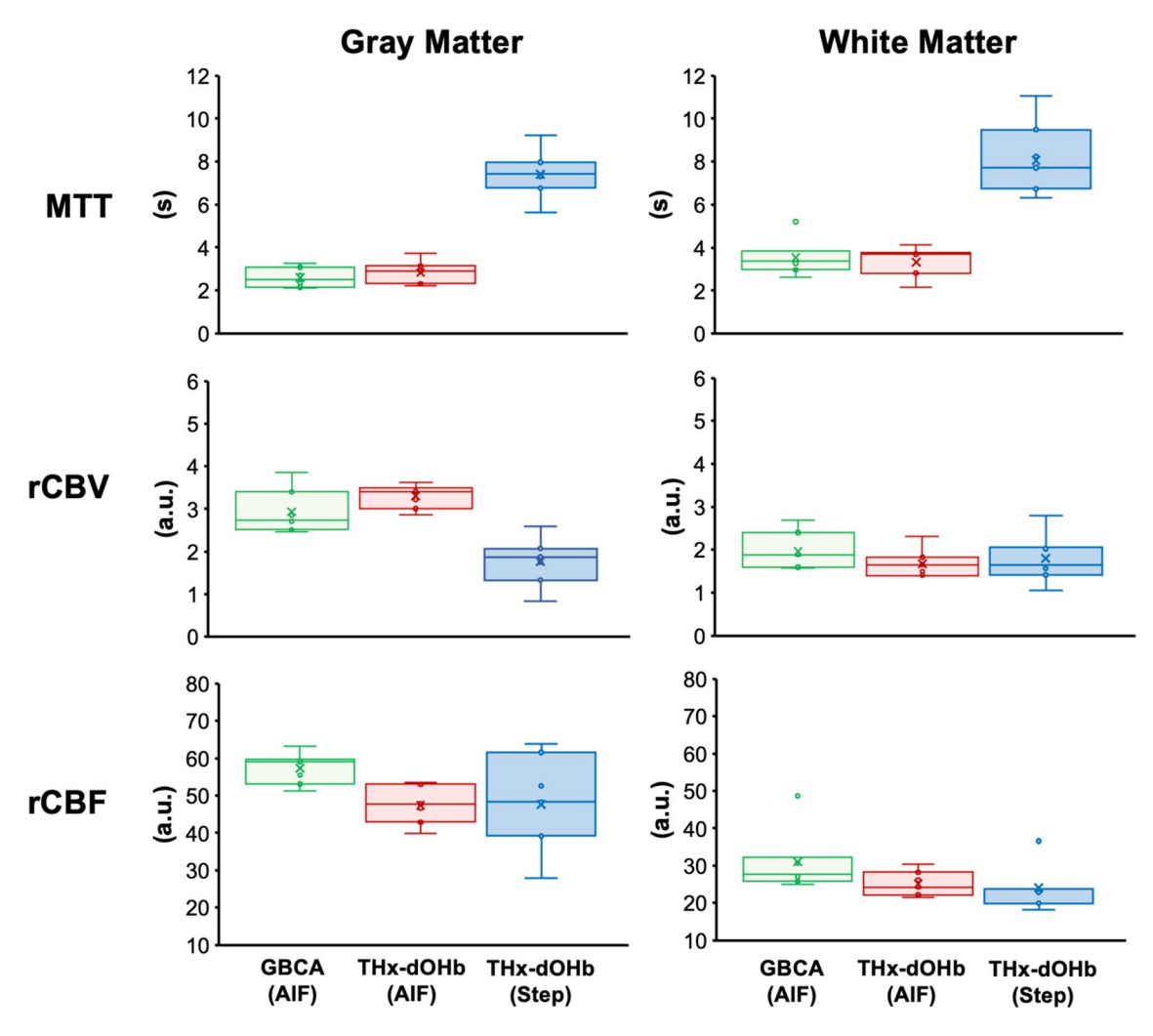


Figure 5. The distribution of the group perfusion metrics in the gray and white matter for the three analyses for the 7 healthy participant group. Note the prolonged MTT from the step analysis (see "Discussion" for an explanation). (GBCA, gadolinium-based contrast agent; THx-dOHb, transient hypoxia induced deoxyhemoglobin; AIF, arterial input function; rCBF, relative cerebral blood flow; rCBV, relative cerebral blood volume; MTT, mean transit time.)

1). A study by Wenzel et al. ³³ found the GM to WM ratio to be \sim 2.1 \pm 0.5 to 1 and Artzi et al. ³⁴ found the GM to WM ratio to be \sim 2.38 to 1 both using DSC-MRI.

Group metrics for MTT

The MTT values for the THx-dOHb-Step analysis are systematically larger than those measured using an AIF and deconvolution. Note that in our model of the THx-dOHb-Step there is a variation in the time of entry of contrast into the voxel (c-D in Fig. 11). We include this ΔR_2^* effect of the distribution of the times of entry of the step SaO₂ change in vessels arriving at the voxel in the calculation of MTT, which results in longer values. For both AIF-deconvolution analyses, the initial entry time of the SaO₂ step change is assumed to be instantaneous for all vessels passing through the voxel. Thus, the longer MTT values from the early arrived contrast is not accounted for (Fig. 2B). Indeed, excluding the time constant of the entry time from the THx-dOHb-Step calculation of MTT results in values falling within the range of the other analyses (Fig. 8) consistent with the shorter MTT values calculated for the GBCA-AIF analyses. The MTT GM to WM ratios were compared between analysis techniques. The GM to WM ratios varied slightly between analyses techniques, nevertheless, the MTT was always longer in WM than in GM (P=0.016). Previously published GM to WM MTT ratios measured by DSC-MRI suggest a ratio ranging between 0.5–0.8 and $1^{29,30,35,36}$, similar to findings of this study, indicating that MTT is consistently longer in WM compared to GM.

The step function

The use of rapid conversion of dOHb to oxyhemoglobin to generate a step function has been previously reported in mechanically ventilated rats by Zhao et al.²² in studying renal hemodynamics. Unfortunately, due to a large apparatus dead space, their *tissue* reoxygenation took 30 s compared to within one breath in our study (Fig. 4 and

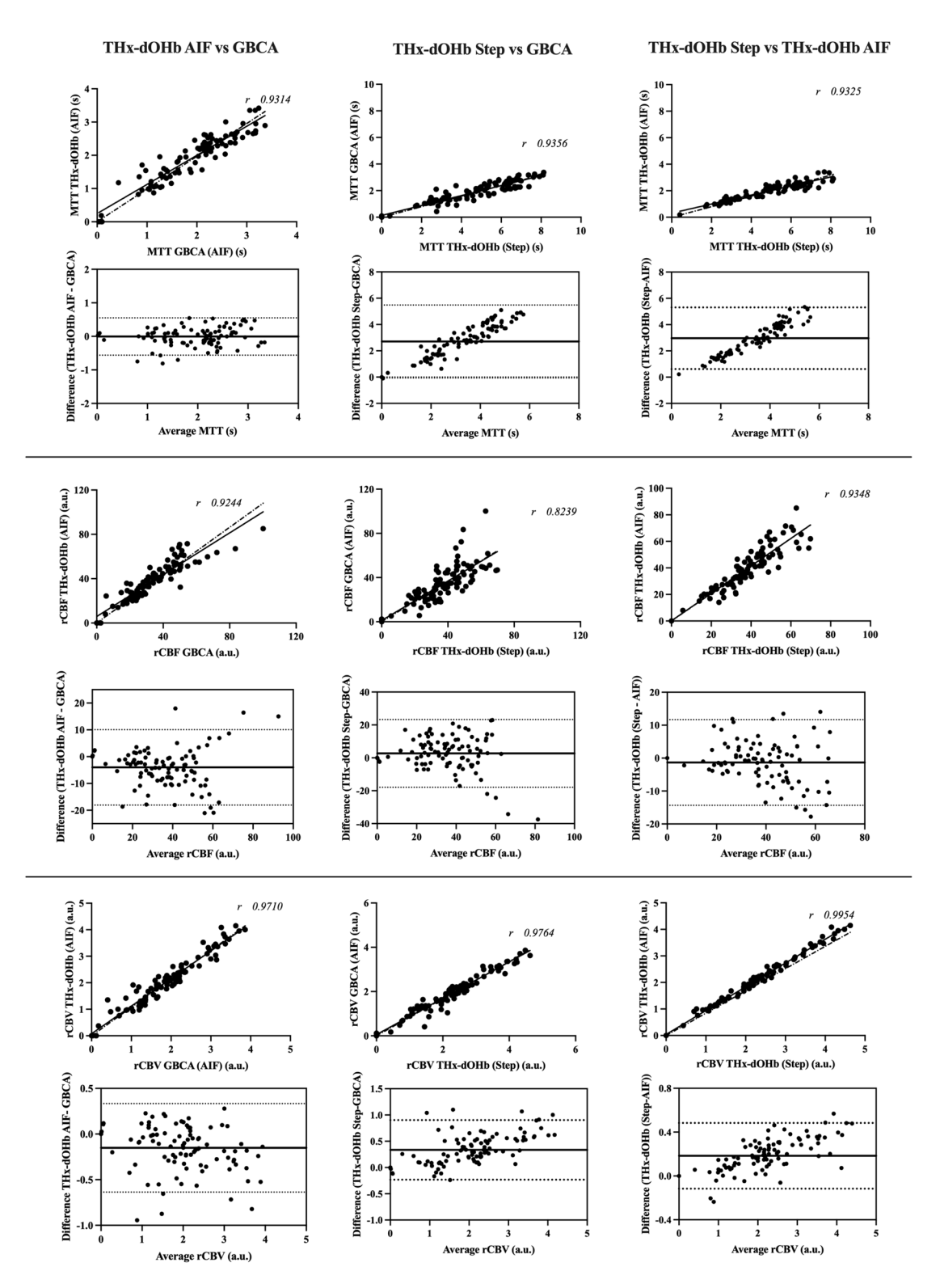


Figure 6. Regional agreement of grouped perfusion metrics between the three analyses. Correlation and Bland–Altman limits of agreement analyses using 100 regions of interest between pairs of perfusion measurements.

Fig. 9). Furthermore, Zhao et al., employed oxygen changes from $10\%~O_2$ (PO $_2$ about 75 mmHg) to $100\%~(PO_2$ about 714 mmHg) for reoxygenation. This high PO $_2$ is unnecessary for resaturation of hemoglobin as it is almost fully saturated at a PO $_2$ of about 90 mmHg 24 . Finally, this high PO $_2$ in the FRC of the rats after reoxygenation resists deoxygenation by dilution of gas in the lungs, which is required for a repeat test. Here, our ability to precisely limit the PO $_2$ in the functional residual capacity to full reoxygenation without hyperoxia has provided

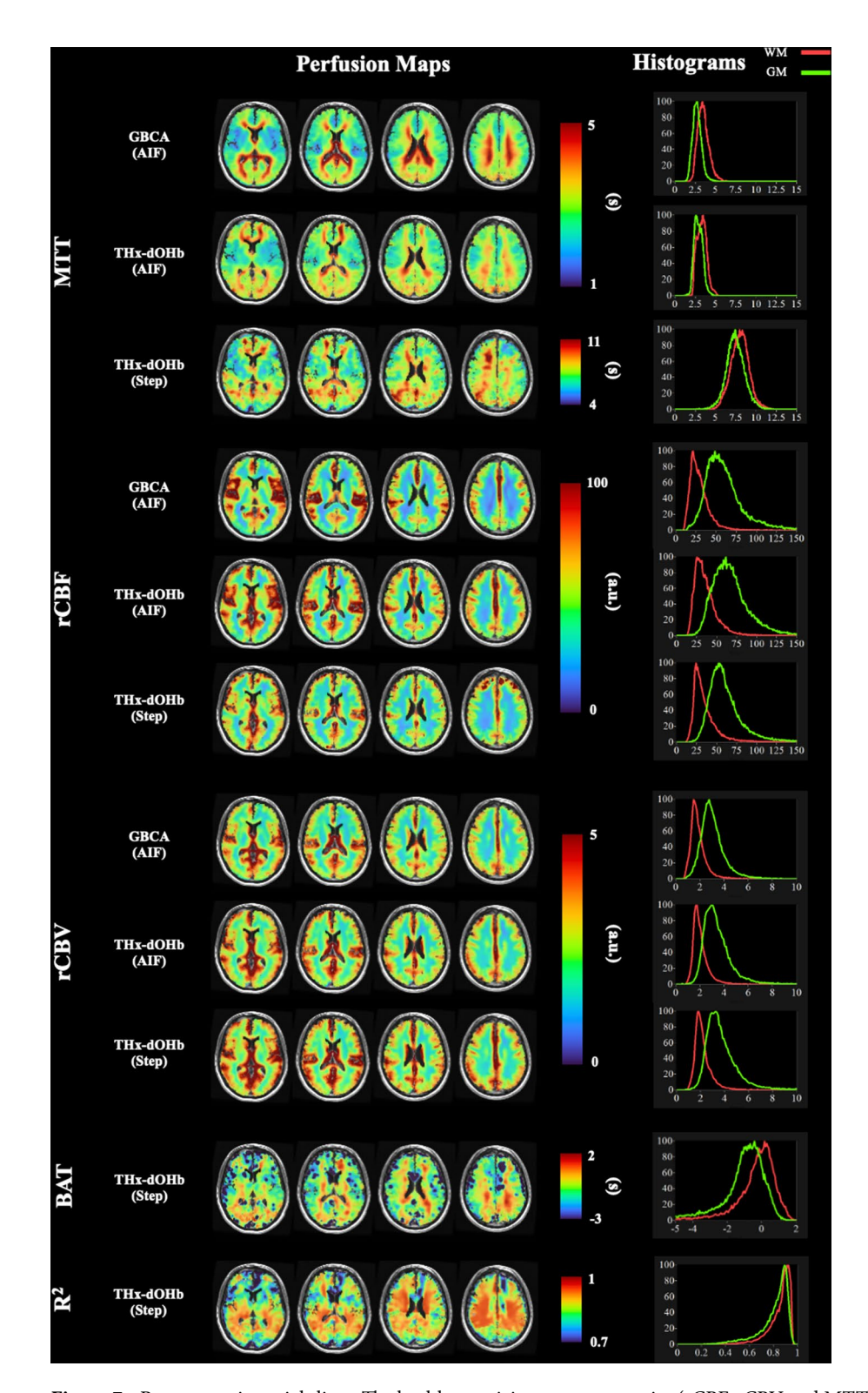


Figure 7. Representative axial slices. The healthy participant group metrics (rCBF, rCBV and MTT) obtained using the three analyses with their associated whole brain histograms for gray matter, GM (red) and white matter, WM (green). The THx-dOHb-Step analysis also provides an R² goodness of fit measure and a blood arrival time relative to the reference cursor time; negative values indicating arrival before the reference cursor time, positive after.

Metric	THx-dOHb-Step	THx-dOHb-AIF	GBCA-AIF	P
MTT	0.95 (0.2)	0.86 (0.11)	0.75 (0.13)	0.11
rCBF	2.22 (0.65)	1.92 (0.32)	1.93 (0.40)	0.44
rCBV	1.96 (0.34)	2.01 (0.30)	1.51 (0.19)	0.008

Table 1. Grouped mean (SD) GM-to-WM ratios.

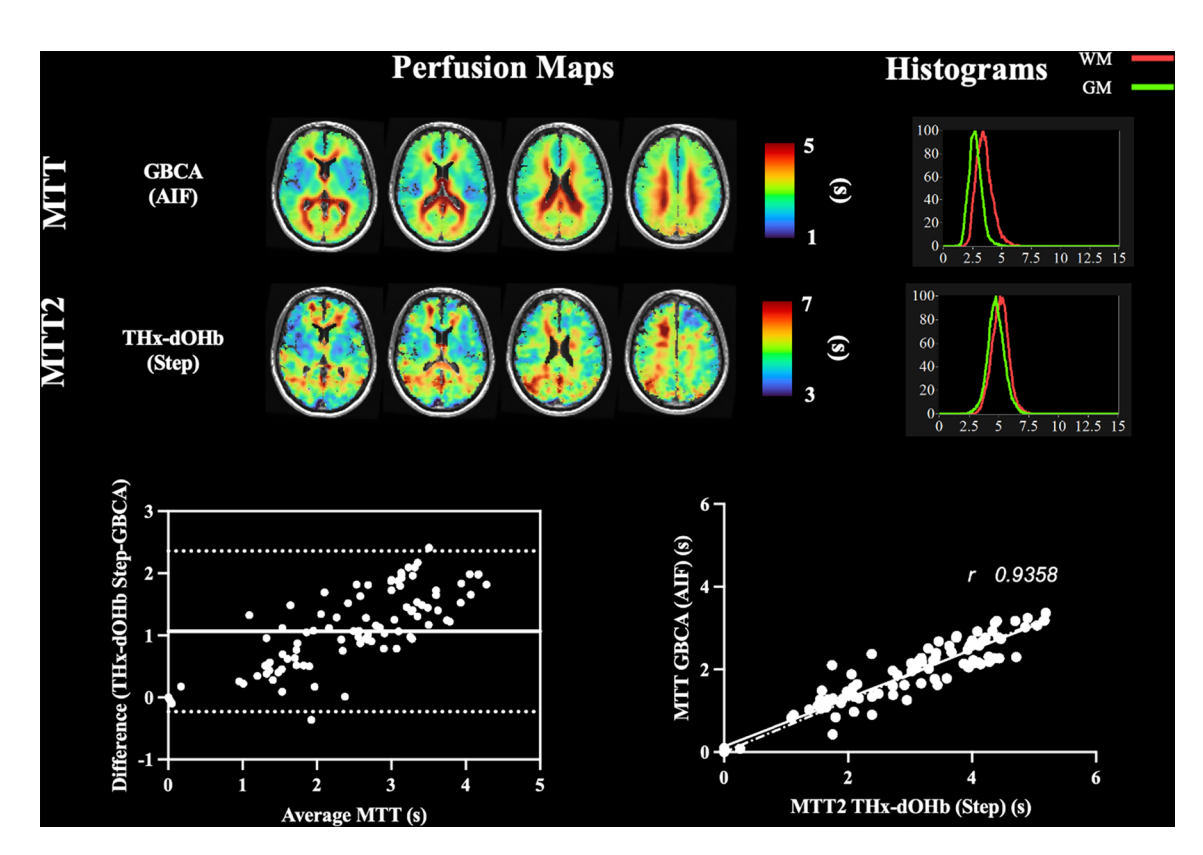


Figure 8. A comparison of group MTT maps and histograms comparing THx-dOHb-Step MTT2 to that of GBCA-AIF, with scatter and Bland–Altman plots. MTT2 is calculated from the THx-dOHb-Step response without the inclusion of the initial entry time constant. The colour scales ranges were adjusted to obtain the highest contrast.

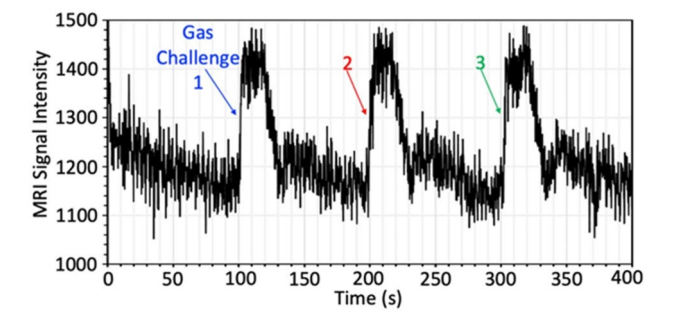


Figure 9. The extent and repeatability of an abrupt step change in lung SaO_2 propagated to the middle cerebral artery. The gas challenge PO_2 alternated between 40 and 95 mmHg; TR of 200 ms; time constants for reoxygenation for challenges 1–3 are 1.21 s, 1.67 s and 2.10 s, respectively. Reproduced from Fig. 2 of Poublanc et al.⁸.

this study the ability to rapidly generate repeat episodes of transient hypoxia and generate step increases in ${\rm SaO_2}$ during resaturation.

Maximizing accuracy and precision of hemodynamic measures by step reoxygenation GBCA arterial Input function

The administration of GBCA and use of indicator dilution kinetics has been a mainstay of hemodynamic measures¹⁸. The pharmacokinetic limitations of this approach follow from the uncontrolled dispersion of the contrast after injection and while flowing to and passing through the heart. No relationship between signal and contrast concentration can be discerned. Hemodynamic measurements must therefore be performed using AIF, deconvolution, and indicator dilution kinetics³⁷.

Deoxyhemoglobin vs GBCA

Deoxyhemoglobin is paramagnetic and has also been used as a contrast agent^{7,8,11,38}. The advances over GBCA are that: (1) dOHb is generated noninvasively and then dissipated with reoxygenation^{8,13}; therefore, repeatable within seconds. By reproducibly targeting [dOHb] in a subject via the RespirAct^{**}, repeated studies are comparable and can facilitate longitudinal hemodynamic monitoring or the comparison of metrics between individuals. (2) dOHb does not leak outside the vessels when measuring blood flow in disorders associated with disruption of the blood–brain-barrier, in contrast to GBCA where leakage correction methods must be applied. Therefore, dOHb should provide more accurate blood flow metrics in the setting of blood–brain-barrier disruption. (3) [dOHb] in the blood and the resulting ΔR_2^* signal can both be measured.

Nevertheless, until now the calculation of hemodynamic parameters has still required designation of an AIF and use of deconvolution calculations based on a hypothetical voxel perfusion model (Fig. 2). Consequently, in this study as in previous studies, GBCA-AIF and THx-dOHb-AIF produce similar hemodynamic measures (Figs. 5, 6 and 7). We suspect that the similarity of the calculated hemodynamic measures from THx-dOHb-AIF and GBCA-AIF analyses results from the deconvolution of a similarly shaped AIF. This concern has been difficult to address as it would apply similarly to any injected contrast agent. Here we confirm that the similarity of hemodynamic measures using THx-dOHb-Step analysis, which is a direct measure, are similar to those derived from THx-dOHb-AIF and GBCA-AIF, which are model based, except for MTT as discussed.

Step [dOHb]

The step reoxygenation radically changes the pharmacokinetic considerations regarding the contrast. With the deconvolution-AIF process, data undergoes considerable averaging, resulting in poor resolution of small differences in measures. On the contrary, with THx-dOHb-Step, the abrupt change in [dOHb] of the blood at the lung is propagated to the MCA and all downstream cerebral vessels (Fig. 9). The increased duration for signal change in a voxel, which produces an increase in MTT, is not due to dispersion of the step change in capillary vessels but reflects the coursing of the contrast through the voxel. We would expect that scanning at a greater field strength and shorter TR would provide an increased time resolution to better fit the Gompertz function.

Study strengths and limitations

The healthy participant group was small and varied in age and sex, so that the results cannot be controlled by either demographic. Data do not reflect the normal range in any specific population. A strength of the study is that we deliberately sampled a wide variety of individuals and focussed on comparison between analyses, whereby each subject served as their own control in the comparison between methods. However, larger studies are required to identify normal ranges of perfusion metrics calculated using the step change in THx-dOHb and to provide a more comprehensive comparison to perfusion metrics calculated from GBCA.

We assumed that the transient changes in PaO₂ do not affect CBF. However, the 60 s exposure to hypoxia may produce an increase in CBF, and act as a confounder for the use of THx-dOHb as a contrast agent, in particular underestimating rCBV and the derived rCBF for the THx-dOHb-AIF analysis. Evidence of such an effect is not conclusive. First, there is considerable variation in the CBF response to hypoxia among individuals. The steady-state increase in CBF as PetO₂ declines from 95 to 40 mmHg varies from as low as 20% to as high as 50% of resting CBF in healthy individuals³⁹. Second, the CBF response to hypoxia is reported to be slow, whereas we found that the time constant for middle cerebral artery velocity changes measured by transcranial Doppler to be about 30 s (unpublished data). Optimally, the time to establish baseline hypoxia should be minimized. Durations to establish hypoxia at 40 mmHg can be arranged to be as short as 12 s (unpublished data) and therefore have minimal effect on CBF.

Future directions

This study was performed at 3 T with a TR of 1500 ms and a voxel size of 3 mm isotropic. While greater time resolution could be provided using a shorter TR, any advantage gained is likely to be at least partially offset by increased noise and limitation of the number of slices scanned. One can also consider utilising larger voxel sizes to reduce the noise at the cost of lower spatial resolution. In this study we analyzed preferentially the second reoxygenation event as it provided sufficient time to come to an equilibrium at full reoxygenation. However, in future studies, a single reoxygenation event may suffice for generating hemodynamic measures, and the effect of additional reoxygenation events could be deployed to assess its effect on signal to noise ratio. Finally, our studies were focused on human brain, but the same step reoxygenation principle may apply to other organs such as in recently investigated animal models of kidney²², heart⁴⁰, and skeletal muscle⁴¹.

We conclude that an input of a step reduction in paramagnetic [dOHb] can generate sufficient ΔR_2^* signal changes in voxels to calculate their resting perfusion metrics using an elementary physiologic vascular model as

shown in Fig. 3. We found that in a group of healthy individuals, average cerebral perfusion metrics and their anatomical distribution corresponded strongly with those calculated using a traditional model-based method requiring identification and deconvolution of an AIF (Fig. 7). The advantages of THx-dOHb-Step analysis over conventional model-based analyses are that it is non-invasive, repeatable, and calculates perfusion metrics directly from the ΔR_2^* signal generated by a more realistic model of blood coursing through a voxel.

Methods

Participants and ethics approval

This study conformed to the standards set by the latest revision of the Declaration of Helsinki and was approved by the Research Ethics Board of the University Health Network (UHN) and Health Canada. Written informed consent to partake in this study was obtained from all participants. We recruited 7 healthy individuals (5 M) between the ages of 24 and 60 (mean \pm SD = 34.4 \pm 16.0 y) by word of mouth. They were non-smokers, not on any medication, and had no known history of neurological or cardiovascular disease. Exclusion criteria consisted of the presence of risk factors for the MRI environment.

Application of contrast agents

The standard sequence of changes in SaO₂ and [dOHb] used for these and other experiments were achieved by controlling the end-tidal partial pressures of oxygen (PetO₂) and carbon dioxide (PetCO₂) using the sequential delivery of inspired gases from a computer-controlled gas blender (RespirAct™; Thornhill Medical, Toronto, Canada) running a prospective targeting algorithm¹⁴. The principles of operation of the RespirAct™ have been previously described^{17,42}. With this targeting approach, the end tidal values have been shown to be equal, within measurement error, to their respective arterial partial pressures^{15,43}. Reduction in pulmonary PO₂ is achieved by inhaling successive tidal volumes of prospectively blended hypoxic gas to dilute the oxygen in the functional residual capacity to target a PetO₂ of 40 mmHg. The reoxygenation step targets the previous baseline PetO₂ of 95 mmHg. We avoid surpassingthe previous baseline PetO₂ on reoxygenation to facilitate rapid reinduction of similar hypoxia-reoxygenation steps.

Participants breathed through a facemask sealed to the face with skin tape (Tegaderm, 3 M, Saint Paul, MN, USA) to exclude all but system-supplied gas. The programmed PetO₂ stimulus consisted of 60 s at 95 mmHg (normoxia), followed by 60 s at 40 mmHg (hypoxia), 20 s at normoxia, followed by 60 s hypoxia and return to normoxia for 60 s (Fig. 10A). PetCO₂ was held constant at the individual's resting value. The entire protocol was used for the THx-dOHb-AIF analysis, but only the terminal step increase in SaO₂ was used for the THx-dOHb-Step analysis. SaO₂ was calculated from the measured PetO₂ and PetCO₂, using the oxyhemoglobin dissociation curve relationship described previously in Eq. (2), assuming a normal pH of 7.4 and a hemoglobin concentration of 130 g/l²⁴. After the completion of the PetO₂ targeting protocol, the participant returned to free breathing of room air for at least 5 min before an intravenous injection of 5 ml at 5 ml/s of Gadovist (Bayer, Canada), with a baseline delay of 20 s prior to injection, and flushed with 30 ml of saline to be used for the GBCA AIF analysis (Fig. 10B).

MRI scanning protocol

The experiments were performed in a 3-Tesla scanner (HDx Signa platform, GE healthcare, Milwaukee, WI, USA) with an 8-channel head coil. The scanning protocol consisted of a high-resolution T1-weighted scan followed by two T2*-weighted acquisitions. The high-resolution T1 scan was acquired using a 3D inversion prepared spoiled fast gradient echo sequence with the following parameters: TI = 450 ms, TR 7.88 ms, TE = 3 ms,

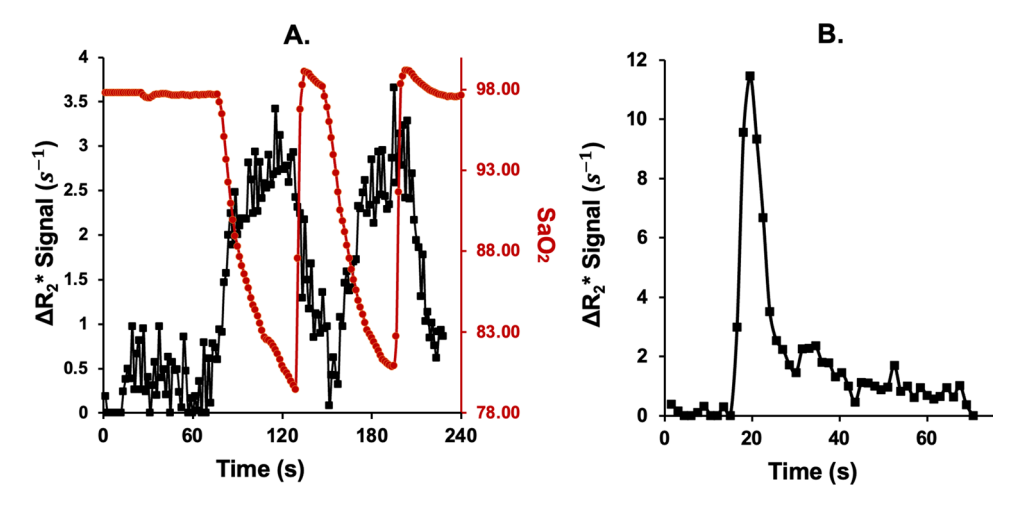


Figure 10. ΔR_2^* signal waveforms for a representative participant in a voxel over the middle cerebral artery (MCA). A) An example of data used for the THx-dOHb-AIF analysis showing the hypoxia-induced changes in SaO₂ (%) (red circles) and the AIF ΔR_2^* signal (black squares) in a representative participant. B) An example of data used for the GBCA AIF analysis showing the AIF ΔR_2^* signal in a representative participant.

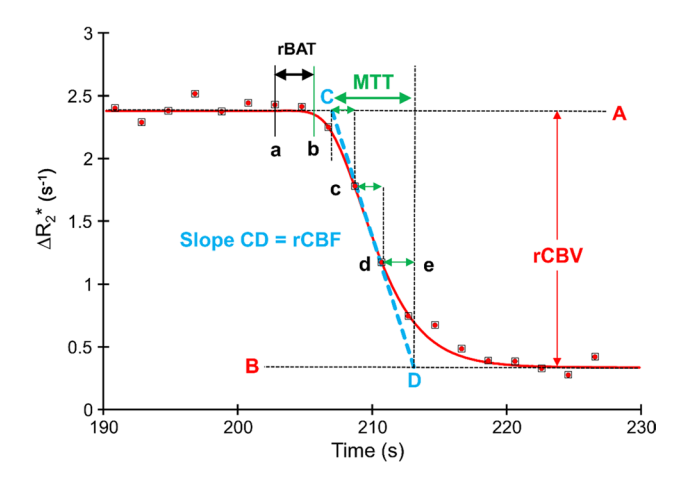


Figure 11. Calculation of hemodynamic variables from the voxel ΔR_2^* signal change following reoxygenation in the lungs. The red filled black squares are the ΔR_2^* signal sampled at TR, with the Gompertz function $S_{fit}(t)$ shown as a red line. The blue dashed line slope is rCBF and its time range is MTT. The amplitude of change represents the rCBV. The geometry of the right angle triangle formed by rCBF, MTT and rCBV verifies the Central Volume Theorem. Further explanation is given in the accompanying text.

flip angle = 12° , voxel size = $0.859 \times 0.859 \times 1$ mm, matrix size = 256×256 , 146 slices, field of view = 220 mm, no interslice gap. Both THx-dOHb and GBCA data acquisitions used a T2*-weighted gradient echoplanar imaging sequence with the following parameters: TR = 1500 ms, TE = 30 ms, flip angle = 73° , 29 slices voxel size = 3 mm isotropic with 64×64 matrix.

Data analysis

The acquired T2*-weighted signal images were volume registered, slice-time corrected and co-registered to the anatomical images using AFNI software (National Institutes of Health, Bethesda, Maryland, Version AFNI_24.0.12 'Caracalla' URL https://afni.nimh.nih.gov) 44 . The acquisitions obtained during both THx-dOHb and GBCA were pre-processed in an identical manner to ensure no bias towards any one scan. The 'spikes' from the dataset were removed and a spatial blur of 5 mm was applied to each dataset using AFNI software. The T2*-weighted signal S(t) acquired during THx-dOHb and GBCA were converted to tissue concentration (ΔR_2^*) using Eq. (3).

$$\Delta R_2 * (t) = (-1/TE) \times \ln\{S(t)/S_0\}$$
 (3)

First, the images from the THx-dOHb and GBCA acquisitions were analyzed using a conventional kinetic model-based approach⁸. The visibly sharpest signal change over a middle cerebral artery was selected as the AIF and a deconvolution-based kinetic model of the type shown in Fig. 2A was used to calculate voxel-wise maps of MTT and rCBV. Standard tracer kinetic modeling was used to calculate MTT and rCBV as stated in Eq. (4).

$$\Delta R_2 * (t) = (rCBV / MTT) \times AIF(t) \otimes R(t) + \beta 1 \times t + \beta 2 + \varepsilon(t)$$
(4)

where t, time; $\beta 1$ and $\beta 2$ account for linear signal drift and baseline t respectively; $\epsilon(t)$ represents the residuals; $R(t) = e^{-(1/MTT)}$ the residue function (Fig. 2A).

The residue function was set equal to 1 at time 0 and 0 at time equal to $5 \times MTT$ and bound between 1 and 8 s. Metrics rCBV and MTT were determined using a least square fitting procedure. rCBF was then calculated as the ratio rCBV/MTT using the central volume theorem, (Fig. 2A). Values of rCBV and rCBF were respectively multiplied by 10 and 50 to obtain easily readable values within the range of absolutes measures.

Second, the voxel-wise analysis of the ΔR_2^* signal during the THx-dOHb step protocol was implemented using a custom analysis program (LabVIEW, National Instruments, Texas) as illustrated in Fig. 4. As Fig. 9 illustrates, the step change in arterial PO₂, via reoxygenation from a hypoxic PetO₂ of approximately 40 to 95 mmHg, produces a step increase in SaO₂, and consequently a step decrease in [dOHb]. The ΔR_2^* signal in a voxel decreases as blood as the increased SaO₂ displaces that at the hypoxic SaO₂. A reference cursor is placed by eye (a in Fig. 11) where the whole brain average ΔR_2^* signal begins to decrease in response to the step increase in SaO₂ and acts as a time reference for all voxels for calculating relative arrival time rBAT.

The THx-dOHb Step analysis, explained in Fig. 11, proceeds as follows: For each voxel, a selected portion of the ΔR_2^* signal response (Fig. 11, red dots in black squares) before and after the reference cursor (a in Fig. 11) is fitted with the Gompertz fit function (Fig. 11, red line) specified in Eq. (5) using the Levenburg-Marquardt algorithm (National Instruments, Texas, LabVIEW), with R-squared indicating the goodness of fit. Fitting a function to the observed ΔR_2^* signal serves to overcome the inherent noise, and a Gompertz function is used to describe the observed ΔR_2^* signal response to the step change in SaO₂.

$$S_{fit}(t) = S_{base} + a \times exp(-b \times exp(-c \times t)); \tag{5}$$

where $S = \Delta R_2^*$; t, time; $S_{fit}(t)$, the fitted ΔR_2^* signal time course of the step response; exp, power of e; S_{base} , the initial value of $S_{fit}(t)$; a, the magnitude of the S decrease; b, the displacement along the time axis; c, the rate of change.

Perfusion metrics rCBV, rCBF and rBAT are all calculated independently as shown in Fig. 11 from the Gompertz function fit to the ΔR_2^* signal step response, $S_{fit}(t)$. MTT is the time range of the line fit (blue dashed line in Fig. 11), which equals rCBV/rCBF. Gompertz function fit parameter "a" measures the complete decrease in the ΔR_2^* step response to calculate rCBV. The start of the ΔR_2^* decrease (Fig. 11, green vertical line) identifies the time where $S_{fit}(t)$ begins to decrease by 2% of rCBV. Relative blood arrival time, rBAT, is calculated as the difference of start time (b) minus reference time (a), with negative values signifying earlier arrival.

The maximum rate of decrease of the ΔR_2^* signal step response is calculated from the $S_{fit}(t)$ parameters as "a×c/e" to measure rCBF, where e is the base of natural logarithms. A line with this slope is drawn through the time of maximum slope, "ln(b)/c" (Fig. 11, blue dashed line). It defines three temporal regions, as indicated by the green arrows in Fig. 11. First, the exponential increase in the rate of decline of the ΔR_2^* signal as the step change in SaO₂ arrives at the voxel until the change has entered the voxel in all capillaries; second, a linear portion of the ΔR_2^* signal decline as all vessels fill with the change in SaO₂ until the change begins to leave the voxel; third, an exponential decay in the rate of decline of the ΔR_2^* signal as the SaO₂ change leaves the voxel. MTT is the sum of the time constants of the first and third temporal regions plus the time taken in the second linear ΔR_2^* signal decrease temporal region. Consequently, MTT satisfies the central volume theorem as the ratio of CBV/CBF. Values of rCBV and rCBF were respectively multiplied by 2 and 200 to obtain easily readable values within the range of absolutes measures (Supplementary Table 1).

The perfusion maps obtained from each analysis were transformed into Montreal Neurological Institute (MNI) space and overlayed onto their respective anatomical images. Analytical processing software, SPM8 (Wellcome Department of Imaging Neuroscience, Institute of Neurology, University College, London, UK, URL https://www.fil.ion.ucl.ac.uk/spm/software/spm8/), was used to segment the anatomical images (T1 weighted) into whole brain cortical supratentorial gray matter (GM) and white matter (WM). Average resting perfusion metrics using all three analyses were calculated for all participants. The MTT, rCBF and rCBV maps for each healthy participant were compiled together to establish average normative ranges for each of the three analyses. This compilation was performed for each metric and analysis by calculating a voxel-by-voxel mean and standard deviations from the co-registered maps in standard space^{45,46}. Additional segmentation into 100 regions of interest (ROIs) was performed by coregistration of T1 images into the Talairach-Tournoux (TT) atlas⁴⁷. Using the TT atlas, ROI between pairs of perfusion metrics was calculated and plotted as scatterplots.

Statistical analysis

Numerical comparisons of the perfusion metrics between the three analyses were not possible for relative values of rCBV and rCBF expressed in arbitrary units. MTT was compared using a two-way ANOVA with factors type of analysis and region (GM vs. WM). To assess the spatial contrast of the maps, we compared the GM to WM ratios using a one-way ANOVA. Both Normality Tests (Shapiro–Wilk) and Equal Variance Tests (Brown-Forsythe) were part of the ANOVA, and correction for multiple comparisons were applied by an all pairwise multiple comparison procedure (Holm-Sidak method). Significant difference for these tests was taken as P < 0.05.

Data availability

Anonymized data will be shared by request from any qualified investigator for purposes such as replicating procedures and results presented in the article provided that data transfer is in agreement with the University Health Network and Health Canada legislation on the general data protection regulation.

Received: 1 October 2023; Accepted: 18 July 2024

Published online: 25 July 2024

References

- 1. Chappell, M. A., Mehndiratta, A. & Calamante, F. Correcting for large vessel contamination in dynamic susceptibility contrast perfusion MRI by extension to a physiological model of the vasculature. *Magn. Reson. Med.* 74, 280–290. https://doi.org/10.1002/mrm.25390 (2015).
- 2. Calamante, F. Arterial input function in perfusion MRI: A comprehensive review. *Prog. Nucl. Magn. Reson. Spectrosc.* **74**, 1–32. https://doi.org/10.1016/j.pnmrs.2013.04.002 (2013).
- Bleeker, E. J., Webb, A. G., van Walderveen, M. A., van Buchem, M. A. & van Osch, M. J. Evaluation of signal formation in local arterial input function measurements of dynamic susceptibility contrast MRI. Magn. Reson. Med. 67, 1324–1331. https://doi.org/ 10.1002/mrm.23120 (2012).
- 4. Shiroishi, M. S. *et al.* Principles of T2 *-weighted dynamic susceptibility contrast MRI technique in brain tumor imaging. *J. Magn. Reson. Imaging* **41**, 296–313. https://doi.org/10.1002/jmri.24648 (2015).
- 5. Sobczyk, O. et al. The choroid plexus as an alternative locus for the identification of the arterial input function for calculating cerebral perfusion metrics using MRI. Am. J. Neuroradiol. 45, 44–50. https://doi.org/10.3174/ajnr.A8099 (2024).
- Coloigner, J. et al. Transient hypoxia model revealed cerebrovascular impairment in anemia using BOLD MRI and near-infrared spectroscopy. J. Magn. Reson. Imaging https://doi.org/10.1002/jmri.27210 (2020).
- 7. Vu, C. et al. Quantitative perfusion mapping with induced transient hypoxia using BOLD MRI. Magn. Reson. Med. 85, 168–181. https://doi.org/10.1002/mrm.28422 (2021).
- 8. Poublanc, J. et al. Perfusion MRI using endogenous deoxyhemoglobin as a contrast agent: Preliminary data. Magn. Reson. Med. 86, 3012–3021. https://doi.org/10.1002/mrm.28974 (2021).
- 9. Lee, D., Le, T. T., Im, G. H. & Kim, S.-G. Whole-brain perfusion mapping in mice by dynamic BOLD MRI with transient hypoxia. J. Cereb. Blood Flow Metab. https://doi.org/10.1177/0271678X221117008 (2022).
- Bhogal, A. A. et al. Quantifying cerebral blood arrival times using hypoxia-mediated arterial BOLD contrast. NeuroImage 261, 119523. https://doi.org/10.1016/j.neuroimage.2022.119523 (2022).

- 11. Sayin, E. S. et al. Investigations of hypoxia-induced deoxyhemoglobin as a contrast agent for cerebral perfusion imaging. Hum. Brain Mapp. 44, 1019–1029. https://doi.org/10.1002/hbm.26131 (2023).
- Schulman, J. B. et al. DSC MRI in the human brain using deoxyhemoglobin and gadolinium—simulations and validations at 3T. Fnimg 2023, 2. https://doi.org/10.3389/fnimg.2023.1048652 (2023).
- Vu, C. et al. Contrast-free dynamic susceptibility contrast using sinusoidal and bolus oxygenation challenges. NMR Biomed. 2024, e5111. https://doi.org/10.1002/nbm.5111 (2024).
- 14. Slessarev, M. et al. Prospective targeting and control of end-tidal CO2 and O2 concentrations. J. Physiol. 581, 1207-1219 (2007).
- 15. Ito, S. et al. Non-invasive prospective targeting of arterial PCO2 in subjects at rest. J. Physiol. 586, 3675-3682 (2008).
- 16. Fierstra, J. et al. Non-invasive accurate measurement of arterial PCO2 in a pediatric animal model. J. Clin. Monit. Comput. 27, 147–155. https://doi.org/10.1007/s10877-012-9403-8 (2013).
- 17. Fisher, J. A., Iscoe, S. & Duffin, J. Sequential gas delivery provides precise control of alveolar gas exchange. *Respir. Physiol. Neurobiol.* 225, 60–69. https://doi.org/10.1016/j.resp.2016.01.004 (2016).
- 18. Meier, P. & Zierler, K. L. On the theory of the indicator-dilution method for measurement of blood flow and volume. *J. Appl. Physiol.* **6**, 731–744 (1954).
- 19. Sayin, E. S. et al. Assessing perfusion in steno-occlusive cerebrovascular disease using transient hypoxia-induced deoxyhemoglobin as a dynamic susceptibility contrast agent. AJNR Am. J. Neuroradiol. 45, 37–43. https://doi.org/10.3174/ajnr.A8068 (2023).
- 20. Vittorio-Stumpo, E. S. S. *et al.* Transient deoxyhemoglobin formation as a contrast for perfusion MRI studies in patients with brain tumors: A feasibility study. *Front. Physiol.* https://doi.org/10.3389/fphys.2024.1238533 (2024).
- 21. Yamaguchi, K., Tsuji, T., Áoshiba, K., Nakamura, H. & Åbe, S. Anatomical backgrounds on gas exchange parameters in the lung. World J. Respirol. 9, 8–29. https://doi.org/10.5320/wjr.v9.i2.8] (2019).
- 22. Zhao, K. et al. Physiological system analysis of the kidney by high-temporal-resolution T2 * monitoring of an oxygenation step response. Magn. Reson. Med. 85, 334–345. https://doi.org/10.1002/mrm.28399 (2021).
- Blockley, N. P. et al. Field strength dependence of R1 and R2 relaxivities of human whole blood to ProHance, vasovist, and deoxyhemoglobin. Magn. Reson. Med. 60, 1313–1320. https://doi.org/10.1002/mrm.21792 (2008).
- 24. Balaban, D. Y. et al. The in-vivo oxyhaemoglobin dissociation curve at sea level and high altitude. Respir. Physiol. Neurobiol. 186, 45–52. https://doi.org/10.1016/j.resp.2012.12.011 (2013).
- Calamante, F. et al. The physiological significance of the time-to-maximum (Tmax) parameter in perfusion MRI. Stroke 41, 1169–1174. https://doi.org/10.1161/STROKEAHA.110.580670 (2010).
- 26. Jespersen, S. N. & Ostergaard, L. The roles of cerebral blood flow, capillary transit time heterogeneity, and oxygen tension in brain oxygenation and metabolism. *J. Cereb. Blood Flow Metab.* 32, 264–277 (2012)
- oxygenation and metabolism. *J. Cereb. Blood Flow Metab.* **32**, 264–277 (2012).

 27. Newbould, R. D. *et al.* Perfusion mapping with multiecho multishot parallel imaging EPI. *Magn. Reson. Med.* **58**, 70–81. https://
- doi.org/10.1002/mrm.21255 (2007).
 Watabe, T. et al. CBF/CBV maps in normal volunteers studied with (15)O PET: A possible index of cerebral perfusion pressure.
- Neurosci. Bull. 30, 857–862. https://doi.org/10.1007/s12264-013-1458-0 (2014).
 29. Grandin, C. B., Bol, A., Smith, A. M., Michel, C. & Cosnard, G. Absolute CBF and CBV measurements by MRI bolus tracking before
- 29. Grandin, C. B., Bol, A., Smith, A. M., Michel, C. & Cosnard, G. Absolute CBF and CBV measurements by MRI bolus tracking before and after acetazolamide challenge: Repeatabilily and comparison with PET in humans. *NeuroImage Orlando, Fla* 26, 525–535. https://doi.org/10.1016/j.neuroimage.2005.02.028 (2005).
- 30. Ibaraki, M. et al. Cerebral vascular mean transit time in healthy humans: A comparative study with PET and dynamic susceptibility contrast-enhanced MRI. J. Cereb. Blood Flow Metab. 27, 404–413. https://doi.org/10.1038/sj.jcbfm.9600337 (2007).
- Asaduddin, M., Do, W.-J., Kim, E. Y. & Park, S.-H. Mapping cerebral perfusion from time-resolved contrast-enhanced MR angiographic data. Magn. Reson. Imaging 61, 143–148. https://doi.org/10.1016/j.mri.2019.05.040 (2019).
- 32. Grüner, İ. M., Paamand, R., Højgaard, L. & Law, I. Brain perfusion CT compared with 15O-H2O-PET in healthy subjects. *EJNMMI Res.* 1, 28. https://doi.org/10.1186/2191-219X-1-28 (2011).
- Wenzel, J. et al. Impaired endothelium-mediated cerebrovascular reactivity promotes anxiety and respiration disorders in mice. Proc. Natl. Acad. Sci. 117, 1753. https://doi.org/10.1073/pnas.1907467117 (2020).
- 34. Artzi, M. et al. Human cerebral blood volume measurements using dynamic contrast enhancement in comparison to dynamic susceptibility contrast MRI. Neuroradiology 57, 671–678. https://doi.org/10.1007/s00234-015-1518-4 (2015).
- 35. Ostergaard, L. *et al.* Cerebral blood flow measurements by magnetic resonance imaging bolus tracking: Comparison with [(15)O] H2O positron emission tomography in humans. *J. Cereb. Blood Flow Metab.* **18**, 935–940. https://doi.org/10.1097/00004647-19980 9000-00002 (1998).
- 36. Helenius, J. et al. Cerebral hemodynamics in a healthy population measured by dynamic susceptibility contrast MR imaging. Acta Radiol. 44, 538–546. https://doi.org/10.1034/j.1600-0455.2003.00104.x (2003).
- Fieselmann, A., Kowarschik, M., Ganguly, A., Hornegger, J. & Fahrig, R. Deconvolution-based CT and MR brain perfusion measurement: Theoretical model revisited and practical implementation details. *Int. J. Biomed. Imaging* 2011, 467563. https://doi. org/10.1155/2011/467563 (2011).
- 38. Sayin, E. S. et al. Transfer function analysis assesses resting cerebral perfusion metrics using hypoxia-induced deoxyhemoglobin as a contrast agent. Front. Physiol. 2023, 14. https://doi.org/10.3389/fphys.2023.1167857 (2023).
- 39. Mardimae, A. et al. The interaction of carbon dioxide and hypoxia in the control of cerebral blood flow. Eur. J. Physiol. 464, 345–351 (2012)
- 40. Yang, H.-J. et al. Free-breathing, motion-corrected, highly efficient whole heart T2 mapping at 3T with hybrid radial-cartesian trajectory. Magn. Reson. Med. 75, 126–136. https://doi.org/10.1002/mrm.25576 (2016).
- 41. Loai, S. et al. Microvascular dysfunction in skeletal muscle precedes myocardial vascular changes in diabetic cardiomyopathy: Sex-dependent differences. Front. Cardiovasc. Med. 2022, 9. https://doi.org/10.3389/fcvm.2022.886687 (2022).
- 42. Fisher, J. A. The CO2 stimulus for cerebrovascular reactivity: Fixing inspired concentrations vs. targeting end-tidal partial pressures. J. Cereb. Blood Flow Metabol. 36, 1004–1011. https://doi.org/10.1177/0271678x16639326 (2016).
- 43. Fierstra, J. et al. End-inspiratory rebreathing reduces the end-tidal to arterial PCO(2) gradient in mechanically ventilated pigs. Intensive Care Med. 37, 1543–1550 (2011).
- 44. Cox, R. W. AFNI: Software for analysis and visualization of functional magnetic resonance neuroimages. *Comput. Biomed. Res.* **29**, 162–173 (1996).
- 45. Sobczyk, O. et al. Assessing cerebrovascular reactivity abnormality by comparison to a reference atlas. *J. Cereb. Blood Flow Metab.* 35, 213–220. https://doi.org/10.1038/jcbfm.2014.184 (2015).
- Sobczyk, O. et al. The reproducibility of cerebrovascular reactivity across MRI scanners. Front. Physiol. 12, 668662–668662. https://doi.org/10.3389/fphys.2021.668662 (2021).
- 47. Nowinski, W. L. The cerefy brain atlases. Neuroinformatics 3, 293-300. https://doi.org/10.1385/NI:3:4:293 (2005).

Author contributions

JAF conceived the study and JD implemented the analyses. DJM selected and reviewed all subjects for suitability. ESS, OS and JP executed the experiments to acquire the data. JD and ESS analysed the data. JD, ESS and JAF wrote the initial draft of the manuscript. All authors participated in the preparation and revision of the final version of the manuscript.

Competing interests

JAF and DJM contributed to the development of the automated end-tidal targeting device, RespirAct™ (Thornhill Medical (TM)) in the company. OS, ESS and JD receive salary support from TM. TM provided no other support for the study. All other authors have no disclosures to report.

Additional information

Supplementary Information The online version contains supplementary material available at https://doi.org/10.1038/s41598-024-68047-w.

Correspondence and requests for materials should be addressed to J.D.

Reprints and permissions information is available at www.nature.com/reprints.

Publisher's note Springer Nature remains neutral with regard to jurisdictional claims in published maps and institutional affiliations.

Open Access This article is licensed under a Creative Commons Attribution-NonCommercial-NoDerivatives 4.0 International License, which permits any non-commercial use, sharing, distribution and reproduction in any medium or format, as long as you give appropriate credit to the original author(s) and the source, provide a link to the Creative Commons licence, and indicate if you modified the licensed material. You do not have permission under this licence to share adapted material derived from this article or parts of it. The images or other third party material in this article are included in the article's Creative Commons licence, unless indicated otherwise in a credit line to the material. If material is not included in the article's Creative Commons licence and your intended use is not permitted by statutory regulation or exceeds the permitted use, you will need to obtain permission directly from the copyright holder. To view a copy of this licence, visit http://creativecommons.org/licenses/by-nc-nd/4.0/.

© The Author(s) 2024